NASA TECHNICAL NOTE

NASA TN D-4195

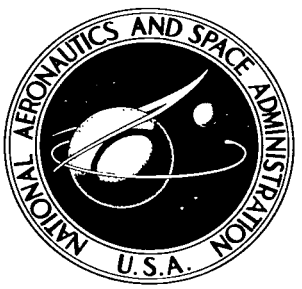




NASA TN D-4195

# A NUMERICAL METHOD FOR STUDYING THE TRANSIENT BLADE MOTIONS OF A ROTOR WITH FLAPPING AND LEAD-LAG DEGREES OF FREEDOM

*by Julian L. Jenkins, Jr.*

*Langley Research Center*
*Langley Station, Hampton, Va.*

NATIONAL AERONAUTICS AND SPACE ADMINISTRATION • WASHINGTON, D. C. • OCTOBER 1967

NASA TN D-4195

# A NUMERICAL METHOD FOR STUDYING THE TRANSIENT BLADE MOTIONS OF A ROTOR WITH FLAPPING AND LEAD-LAG DEGREES OF FREEDOM

By Julian L. Jenkins, Jr.

Langley Research Center
Langley Station, Hampton, Va.

NATIONAL AERONAUTICS AND SPACE ADMINISTRATION

For sale by the Clearinghouse for Federal Scientific and Technical Information
Springfield, Virginia 22151 – CFSTI price $3.00

# A NUMERICAL METHOD FOR STUDYING THE TRANSIENT BLADE MOTIONS OF A ROTOR WITH FLAPPING AND LEAD-LAG DEGREES OF FREEDOM

By Julian L. Jenkins, Jr.
Langley Research Center

## SUMMARY

The equations of motion for the fully articulated rotor system (i.e., rigid blade with flapping and lead-lag degrees of freedom) are derived and the procedure used to obtain a numerical solution of the nonlinear coupled equations of motion is outlined. The equations can be applied to a rotor system with blades of any airfoil section, mass distribution, twist, taper, and root cutout. The hinge geometry is variable; however, the restraints considered require that the lag hinge be coincident with or outboard of the flapping hinge. Two-dimensional stall and compressibility effects can be accounted for.

Stability boundaries are defined in terms of an absolute limit (i.e., hinge motion amplitudes greater than $90^{\circ}$) for varying blade mass constants as a function of the initial azimuth position for introducing a disturbance. In addition, a boundary is presented which is based on the criterion of neutral spring forces in the forward quadrants of the rotor when the blade is released with an initial flapping-angle displacement at an initial azimuth angle of $90^{\circ}$. This boundary is thus a measure of the tip-speed ratio at which the nonlinear spring forces in the forward quadrants are approximately zero. A comparison of this boundary with one based on a maximum flapping amplitude limit of $15^{\circ}$ for a 30-ft/sec (9.14-m/sec) vertical gust indicates good correlation.

## INTRODUCTION

The problem of defining rotor-blade-motion stability and predicting response to disturbances has been a subject of study for many years. These studies have produced numerous and ofttimes contradictory results, depending on the simplifying assumptions made in order to handle the complicated rotor dynamic system. Such assumptions generally leave the applicability of the results subject to question, particularly at extreme operating conditions.

Although most investigations have shown the rotor flapwise motion to be very stable below tip-speed ratios of 1.0 (see, for example, refs. 1 to 3), there have been indications that inclusion of the nonlinear coupling of flapwise and chordwise blade motions might

introduce marginal stability characteristics of the rotor (see ref. 4). In any event, continuing efforts to increase the operating speed of both the pure helicopter and the compound configurations require a more exacting treatment of the nonlinear dynamics of the rotor system inasmuch as it becomes progressively more difficult to prevent excessive blade motions at high tip-speed ratios and under maneuvering conditions at moderate tip-speed ratios. Also, the transient response of the rotor to gusts is of more importance at higher tip-speed ratios because of increased rotor response sensitivity.

In an effort to obtain further insight into the problems of blade-motion stability and to evaluate the possibility of unstable or excessive blade motions as a result of nonlinear coupling of flapwise and chordwise motions, the rigid-body equations of motion for the fully articulated rotor system (i.e., rigid blades with flapping and lead-lag degrees of freedom) have been derived and programed for obtaining a numerical solution on a digital computer. This report presents a description of the method of derivation of the equations and the procedures used to obtain solutions. In addition, the results of a study of the blade-motion stability and response characteristics of the fully articulated rotor system are presented and discussed.

## SYMBOLS

| | |
|---|---|
| $a$ | speed of sound, ft/sec (m/sec) |
| $a_F$ | resultant blade-element acceleration about flapping hinge, ft/sec$^2$ (m/sec$^2$) |
| $a_L$ | resultant blade-element acceleration about lag hinge, ft/sec$^2$ (m/sec$^2$) |
| $A_0$ | collective pitch angle at blade root, average value of instantaneous blade-root pitch angle around azimuth, deg |
| $A_1, B_1$ | coefficients of $-\cos\psi$ and $-\sin\psi$, respectively, in expression for $\theta$; therefore, lateral and longitudinal cyclic-pitch angles, respectively, deg |
| $b$ | number of blades |
| $B$ | tip-loss factor (assumed equal to 0.97 herein); blade elements outboard of radius $BR$ are assumed to have profile drag but no lift |
| $c$ | blade section chord, ft (m) |
| $c_{d,o}$ | section profile-drag coefficient |

$c_l$ section lift coefficient

$C_{d,F}$ flapping damper coefficient, lb-ft-sec/rad (N-m-sec/rad)

$C_{d,L}$ lag damper coefficient, lb-ft-sec/rad (N-m-sec/rad)

$C_{M_D}$ aerodynamic drag moment coefficient in lead-lag equation of motion at given blade azimuth angle

$C_{M_T}$ aerodynamic thrust moment coefficient in flapping equation of motion at given blade azimuth angle

dD incremental drag force on blade element, lb (N)

$e_1$ offset of center line of flapping hinge from center line of rotor shaft, ft (m)

$e_2$ offset of center line of lead-lag hinge from center line of flapping hinge, ft (m)

$e_t$ offset of center line of lead-lag hinge from center line of rotor shaft, $e_1 + e_2$, ft (m)

g gravitational acceleration, ft/sec$^2$ (m/sec$^2$)

$I_e$ mass moment of inertia of hub arm $e_2$ about flapping hinge, $\int_{e_1}^{e_t} m(r - e_1)^2 dr$, slug-ft$^2$ (kg-m$^2$)

$I_h$ mass moment of inertia of blade about lead-lag hinge, $\int_{e_t}^{R} m(r - e_t)^2 dr$, slug-ft$^2$ (kg-m$^2$)

$K_{SF}$ flapping spring constant, lb-ft/rad (N-m/rad)

$K_{SL}$ lag spring constant, lb-ft/rad (N-m/rad)

dL incremental lift force on blade element, lb (N)

m mass of blade per unit of radius, slugs/ft (kg/m)

$M_A$ aerodynamic-force moment, lb-ft (N-m)

$M_d$ damper moment, lb-ft (N-m)

$M_I$ inertia-force moment, lb-ft (N-m)

$M_S$ spring-restraint moment, lb-ft (N-m)

$M_W$ weight moment, lb-ft (N-m)

$M'_W$ weight moment of blade at zero angular displacement, $\int_{e_t}^{R} mg(r - e_t)dr$, lb-ft (N-m)

$M'_{W,e}$ weight moment of hub arm $e_2$ at zero angular displacement, $\int_{e_1}^{e_t} mg(r - e_1)dr$, lb-ft (N-m)

$M_{(x,\psi)}$ local Mach number $U/a$ at a given radial station and azimuth angle

dN resultant aerodynamic force on blade element perpendicular to blade lag plane, lb (N)

dP component of aerodynamic force on blade element perpendicular to blade-span axis and in the blade lag plane, lb (N)

r distance measured along blade from axis of rotation to blade element, ft (m)

$r_c$ radius of blade root pocket cutout (i.e., radius at which lifting surface of blade begins), ft (m)

$r_F$ radial distance from flapping-hinge $Y_F$-axis to mass element, measured in plane perpendicular to hinge axis, ft (m)

R total radius of undeflected blade, ft (m)

t time, sec

u nondimensional resultant velocity at local blade element, $U/\Omega R$

$U$ resultant velocity perpendicular to blade-span axis at blade element, ft/sec (m/sec)

$U_P$ component at blade element of resultant velocity perpendicular to both the blade-span axis and $U_T$, ft/sec (m/sec)

$U_T$ component at blade element of resultant velocity perpendicular to the blade-span axis and in the $X_L$-$Y_L$ plane, ft/sec (m/sec)

$V$ velocity along flight path, ft/sec (m/sec)

$W_b$ blade weight, $\int_{e_t}^{R} mg\, dr$, lb (N)

$W_e$ weight of hub arm $e_2$, $\int_{e_1}^{e_t} mg\, dr$, lb (N)

$x$ ratio of blade-element radius to rotor-blade radius, $r/R$

$x_1 = e_1/R$

$x_2 = e_2/R$

$x_c = r_c/R$

$x_t = e_t/R$

$X_e, Y_e, Z_e$ earth reference axes

$X_F, Y_F, Z_F$ flapping axes

$X_L, Y_L, Z_L$ lag axes

$X_S, Y_S, Z_S$ shaft axes

$z_{tip}$ vertical displacement of blade tip from $X_S$-$Y_S$ plane, ft (m)

$\alpha_r$ blade-element angle of attack, measured from line of zero lift, deg

$\alpha_s$ angle between shaft axis and plane perpendicular to flight path, positive when axis is pointing rearward, deg

$\beta$ blade-flapping-hinge angle at particular azimuth position, rad

$\dot{\beta},\ddot{\beta}$ first and second derivatives of $\beta$ with respect to time

$\overline{\beta},\overline{\overline{\beta}}$ first and second derivatives of $\beta$ with respect to azimuth angle $\psi$

$\beta_{(90-270)}$ blade-flapping-hinge angle in azimuth range from $90^{o}$ to $270^{o}$, rad

$\gamma'$ mass constant of rotor blade, $\frac{\rho c R^4}{I_h}$

$\delta_3$ blade-flapping-hinge cant angle, deg

$\epsilon = \frac{W_b R^2}{g I_h}$

$\zeta$ blade leading angle at particular azimuth position, rad

$\dot{\zeta},\ddot{\zeta}$ first and second derivatives of $\zeta$ with respect to time

$\overline{\zeta},\overline{\overline{\zeta}}$ first and second derivatives of $\zeta$ with respect to azimuth angle $\psi$

$\eta = \frac{M'_W R}{g I_h}$

$\eta_e = \frac{M'_{W,e} R}{g I_h}$

$\Theta$ rotor pitch attitude referred to earth axes, deg

$\theta$ instantaneous blade-section pitch angle, $A_0 - A_1 \cos\psi - B_1 \sin\psi + \theta_1 x$, deg

$\theta_1$ difference between root and tip geometric pitch angles, positive when tip angle is larger, deg

$\lambda$ inflow ratio, $\frac{V \sin\alpha_s - \nu}{\Omega R}$

$\Lambda = I_e/I_h$

$\mu$ tip-speed ratio, $\frac{V \cos\alpha_s}{\Omega R}$

$\nu$ induced inflow velocity at rotor, positive downward, ft/sec (m/sec)

$\rho$ mass density of air, slugs/ft$^3$ (kg/m$^3$)

$\sigma$ rotor solidity, $bc/\pi R$

$\phi$ inflow angle at blade element in plane perpendicular to blade-span axis, $\tan^{-1}\frac{U_P}{U_T}$, deg

$\Phi$ rotor bank angle referred to earth axes, deg

$\psi$ blade azimuth angle, measured from downwind position in direction of rotation, deg or rad as indicated

$\Omega$ rotor angular velocity, $d\psi/dt$, rad/sec

Subscripts:

o initial condition

F referred to flapping axes

L referred to lag axes

max maximum

s referred to shaft axes

x,y,z components in x-, y-, and z-directions, respectively

## METHOD OF ANALYSIS

The equations of motion for a blade with full articulation are derived by equating the moments about the hinge points to zero. The general moment expression for the two hinge points considered herein is as follows:

$$M_I + M_A + M_W + M_S + M_d = 0 \quad (1)$$

where

$M_I$ inertia moment

$M_A$ aerodynamic-force moment

$M_W$ weight moment

$M_S$ spring-restraint moment

$M_d$ damper moment

The two differential equations required are obtained by writing the expressions for the individual moments of equations (1).

## Reference Axes

The basic hub system considered herein is illustrated in figure 1. Included also are the axes used to derive the equations of motion. The basic reference axes are the shaft axes, which consist of a nonrotating, right-hand, orthogonal system with the $Z_S$-axis coincident with the shaft axis and the $X_S$-axis in the plane of the velocity vector V, and the $Z_S$-axis. The $Y_S$-axis is perpendicular to the $X_S$- and $Z_S$-axes and is positive in the direction of $\psi = 90^o$ on the advancing side of the rotor disk (see fig. 1).

The additional axes are the flapping axes and lag axes which are rotating, right-hand orthogonal axes with origins at the flapping hinge and lagging hinge, respectively. The flapping axes consist of an $X_F$-axis perpendicular to the flapping-hinge axis and in the $X_S$-$Y_S$ plane, a $Y_F$-axis coincident with the flapping-hinge axis, and a $Z_F$-axis parallel to the $Z_S$-axis and perpendicular to the $X_F$- and $Y_F$-axes. The lag axes consist of an $X_L$-axis coincident with the hub arm $e_2$, a $Y_L$-axis perpendicular to the $X_L$-axis and the lag-hinge axis, and a $Z_L$-axis coincident with the lag-hinge axis. It should be noted that the lead-lag angle $\zeta$ is measured in the $X_L$-$Y_L$ plane and that the flapping angle $\beta$ is the angle between the $X_F$-axis and the line formed by the intersection of the blade plane $X_L$-$Y_L$ and the $X_F$-$Z_F$ plane.

## Lead-Lag Degree of Freedom

The lead-lag equation-of-motion expressions for moments acting about the lag hinge are given in the following sections.

Inertia moment.- The inertia-moment expression may be written as

$$M_{I,L} = -\int_{e_t}^{R} m(r - e_t)a_L \, dr \tag{2}$$

where $a_L$ is the component about the lag hinge of the total acceleration of a mass element.

A detailed derivation is not presented herein; however, the procedure used was to write the expression for the displacement of a mass element in terms of the shaft-axes

coordinates and to obtain the first and second time derivatives of the expression. Then by use of appropriate coordinate transformation matrices, the total acceleration may be expressed as acceleration components referred to the lag axes. These components may then be resolved into the desired resultant component perpendicular to the blade span. This procedure yields the following expression for $a_L$:

$$a_L = \ddot{\zeta}(r - e_t) - 2\Omega\dot{\beta}\left[(r - e_t)\cos^2(\zeta + \delta_3)\sin\beta + e_2\cos\delta_3\cos(\zeta + \delta_3)\sin\beta\right]$$

$$+ \dot{\beta}^2\left[(r - e_t)\sin(\zeta + \delta_3)\cos(\zeta + \delta_3) + e_2\cos\delta_3\sin(\zeta + \delta_3)\right]$$

$$+ \Omega^2\left[(e_1 + e_2\cos\beta)\cos\delta_3\cos\beta\sin(\zeta + \delta_3) - e_t\sin\delta_3\cos(\zeta + \delta_3)\right]$$

$$- \Omega^2(r - e_t)\sin(\zeta + \delta_3)\cos(\zeta + \delta_3)\sin^2\beta \qquad (3)$$

Substituting equation (3) into equation (2) and integrating yields

$$M_{I,L} = -I_h\ddot{\zeta} + 2\Omega\dot{\beta}I_h\cos^2(\zeta + \delta_3)\sin\beta + 2\Omega\dot{\beta}\frac{M_W'}{g}e_2\cos\delta_3\cos(\zeta + \delta_3)\sin\beta$$

$$- \dot{\beta}^2 I_h\sin(\zeta + \delta_3)\cos(\zeta + \delta_3) - \dot{\beta}^2\frac{M_W'}{g}e_2\cos\delta_3\sin(\zeta + \delta_3)$$

$$- \Omega^2\frac{M_W'}{g}\left[(e_1 + e_2\cos\beta)\cos\delta_3\cos\beta\sin(\zeta + \delta_3) - e_t\sin\delta_3\cos(\zeta + \delta_3)\right]$$

$$+ \Omega^2 I_h\sin(\zeta + \delta_3)\cos(\zeta + \delta_3)\sin^2\beta \qquad (4)$$

Aerodynamic-force moment.- The aerodynamic-force moment about the lag hinge is obtained by resolving the element lift and drag forces into a resultant force about the lag hinge. It should be noted that the aerodynamic forces are obtained by using a quasi-static, independent-element analysis. Figure 2 illustrates the forces acting on the element. The element lift force is

$$dL = \frac{1}{2}\rho U^2 c_l c\, dr \qquad (5)$$

and the element drag force is

$$dD = \frac{1}{2}\rho U^2 c_{d,o} c\, dr \qquad (6)$$

The desired resultant force $dP$ is given by

$$dP = dD\cos\phi - dL\sin\phi \qquad (7)$$

From figure 3, the aerodynamic-force moment is

$$M_{A,L} = -\int_{r_c}^{R} (r - e_t) dP \tag{8}$$

Substituting equations (5), (6), and (7) into equation (8) yields

$$M_{A,L} = \int_{r_c}^{BR} \frac{1}{2} \rho U^2 c_l c \, (r - e_t) \sin \phi \, dr - \int_{r_c}^{R} \frac{1}{2} \rho U^2 c_{d,o} c (r - e_t) \cos \phi \, dr \tag{8a}$$

It is assumed that $r_c$ is equal to or greater than $e_t$ so that no aerodynamic-moment contributions are included for the blade spar inboard of the root pocket cutout. In addition, the integration of the lift integral contains the tip-loss factor B so that lift forces beyond BR are neglected.

The additional expressions required to evaluate equation (8a) are as follows:

$$U^2 = U_T^2 + U_P^2 \tag{9}$$

where

$$U_T = \Omega(r - e_t)\cos \beta + \Omega e_t \cos \zeta \cos \beta + \Omega e_1 \cos \delta_3 \cos(\zeta + \delta_3)(1 - \cos \beta) + \dot{\zeta}(r - e_t)$$

$$+ \Omega R \mu \left[\cos(\psi - \delta_3)\sin(\zeta + \delta_3)\cos \beta + \sin(\psi - \delta_3)\cos(\zeta + \delta_3)\right]$$

$$+ \Omega R \lambda \sin(\zeta + \delta_3)\sin \beta \tag{9a}$$

and

$$U_P = \Omega R \lambda \cos \beta - \Omega R \mu \cos(\psi - \delta_3)\sin \beta - \Omega(r - e_t)\sin(\zeta + \delta_3)\sin \beta$$

$$- \dot{\beta}(r - e_t)\cos(\zeta + \delta_3) - \dot{\beta} e_2 \cos \delta_3 - \Omega e_t \sin \delta_3 \sin \beta \tag{9b}$$

$$\phi = \tan^{-1} \frac{U_P}{U_T} \tag{10}$$

$$\alpha_r = \theta + \phi \tag{11}$$

$$M_{(x,\psi)} = \frac{U}{a} \tag{12}$$

Expressions (11) and (12) are used to determine the section lift and drag coefficients required in equation (8a). The lift and drag coefficients are functions of section

angle of attack and Mach number; thus, compressibility and two-dimensional stall effects may be taken into account for arbitrary airfoil sections.

It should be noted that the section angle of attack (eq. (11)) and the velocities $U_T$ and $U_P$ are derived with respect to the lag axes, and consequently, the pitch change due to the flapping and lag position is taken into account. In order to decouple the blade pitch from the flapping and lag displacement, the following expression may be used for the section angle of attack:

$$\alpha_r = \theta + \phi + \Delta\theta \tag{13}$$

where

$$\Delta\theta = \tan^{-1}(\sin \zeta \tan \beta) \tag{13a}$$

Weight moment.- The expression for the in-plane weight moments is obtained by first orienting the gravity vector with respect to the shaft and then determining the component about the lag hinge from the appropriate coordinate transformations. As illustrated in figure 4, the gravity vector must be transformed through the angles $\Theta$ and $\Phi$ to obtain components referred to the shaft axes. The expression for the transformation is

$$\begin{Bmatrix} g_x \\ g_y \\ g_z \end{Bmatrix}_s = \begin{bmatrix} \cos\Theta & 0 & -\sin\Theta \\ \sin\Phi\sin\Theta & \cos\Phi & \sin\Phi\cos\Theta \\ \sin\Theta\cos\Phi & -\sin\Phi & \cos\Phi\cos\Theta \end{bmatrix} \begin{Bmatrix} 0 \\ 0 \\ -g \end{Bmatrix} \tag{14}$$

By appropriate coordinate transformations, the gravitational acceleration about the lag hinge may be shown to be

$$\begin{aligned} g_L = {} & g \sin(\zeta + \delta_3)\sin\beta\cos\Phi\cos\Theta \\ & - g\left[\cos(\psi - \delta_3)\sin(\zeta + \delta_3)\cos\beta + \sin(\psi - \delta_3)\cos(\zeta + \delta_3)\right]\sin\Theta \\ & + g\left[\sin(\psi - \delta_3)\sin(\zeta + \delta_3)\cos\beta - \cos(\psi - \delta_3)\cos(\zeta + \delta_3)\right]\sin\Phi\cos\Theta \end{aligned} \tag{15}$$

The expression for the weight moment about the lag hinge is

$$M_{W,L} = \int_{e_t}^{R} m g_L (r - e_t)\,dr \tag{16}$$

Substituting equation (15) into equation (16) and integrating yields the following expression for the weight moment:

$$M_{W,L} = M'_W \Big\{ \sin(\zeta + \delta_3)\sin\beta\cos\Phi\cos\Theta - \left[\cos(\psi - \delta_3)\sin(\zeta + \delta_3)\cos\beta + \sin(\psi - \delta_3)\cos(\zeta + \delta_3)\right]\sin\Theta + \left[\sin(\psi - \delta_3)\sin(\zeta + \delta_3)\cos\beta - \cos(\psi - \delta_3)\cos(\zeta + \delta_3)\right]\sin\Phi\cos\Theta \Big\} \quad (17)$$

Spring-restraint moment.- The spring moment which is included in the in-plane equation of motion may be used to represent either an actual spring restraint or to simulate the structural stiffness of a hingeless rotor.

The expression for the moment is

$$M_{S,L} = -K_{SL}\zeta \quad (18)$$

where $K_{SL}$ is the lag spring constant.

Damper moment.- The damper-moment expression has been included to represent either a viscous damping moment or simulated structural damping.

The moment is defined as

$$M_{d,L} = -C_{d,L}\dot{\zeta} \quad (19)$$

where $C_{d,L}$ is the lag damper coefficient.

Lead-lag equation of motion.- The expressions for the moments about the lag hinge have been derived in the preceding sections. Substitution of the five terms (eqs. (4), (8a), (17), (18), and (19)) into equation (1) yields the following equation of motion for the lag degree of freedom:

$$-I_h\ddot{\zeta} + I_h\Omega^2\sin(\zeta + \delta_3)\cos(\zeta + \delta_3)\sin^2\beta - I_h\dot{\beta}^2\sin(\zeta + \delta_3)\cos(\zeta + \delta_3) + 2I_h\Omega\dot{\beta}\cos^2(\zeta + \delta_3)\sin\beta$$
$$- \frac{M'_W}{g}\Omega^2 e_1\cos\delta_3\cos\beta\sin(\zeta + \delta_3) + \frac{M'_W}{g}\Omega^2 e_t\sin\delta_3\cos(\zeta + \delta_3) - \frac{M'_W}{g}\Omega^2 e_2\cos\delta_3\cos^2\beta\sin(\zeta + \delta_3)$$
$$- \frac{M'_W}{g}\dot{\beta}^2 e_2\cos\delta_3\sin(\zeta + \delta_3) + 2\frac{M'_W}{g}\Omega\dot{\beta}e_2\cos\delta_3\cos(\zeta + \delta_3)\sin\beta - M'_W\Big\{\left[\cos(\psi - \delta_3)\sin(\zeta + \delta_3)\cos\beta\right.$$
$$\left. + \sin(\psi - \delta_3)\cos(\zeta + \delta_3)\right]\sin\Theta - \left[\sin(\psi - \delta_3)\sin(\zeta + \delta_3)\cos\beta - \cos(\psi - \delta_3)\cos(\zeta + \delta_3)\right]\sin\Phi\cos\Theta$$
$$- \sin(\zeta + \delta_3)\sin\beta\cos\Phi\cos\Theta\Big\} + \int_{r_c}^{BR}\frac{1}{2}\rho U^2 c_l\, c\sin\phi(r - e_t)dr - \int_{r_c}^{R}\frac{1}{2}\rho U^2 c_{d,o}\, c\cos\phi(r - e_t)dr - K_{SL}\zeta - C_{d,L}\dot{\zeta} = 0 \quad (20)$$

Equation (20) is the dimensional equation of motion. It may be nondimensionalized by dividing by $-I_h\Omega^2$ and substituting the following expressions:

$$\left.\begin{array}{llll} \dot{\zeta} = \dfrac{d\psi}{dt}\dfrac{d\zeta}{d\psi} = \Omega\bar{\zeta} & e_1 = x_1 R & U = u\Omega R & \dfrac{W_b R^2}{gI_h} = \epsilon \\ \ddot{\zeta} = \Omega^2\bar{\bar{\zeta}} & e_2 = x_2 R & \dfrac{\rho c R^4}{I_h} = \gamma' & \dfrac{M'_W R}{gI_h} = \eta \\ \dot{\beta} = \Omega\bar{\beta} & e_t = x_t R & & \\ \ddot{\beta} = \Omega^2\bar{\bar{\beta}} & r = xR & \dfrac{I_e}{I_h} = \Lambda & \dfrac{M'_{W,e} R}{gI_h} = \eta_e \\ & r_c = x_c R & & \end{array}\right\} \quad (21)$$

The nondimensional lead-lag equation of motion is

$$\begin{aligned} &\bar{\bar{\zeta}} - \left[\sin^2\beta - \bar{\beta}^2\right]\sin(\zeta + \delta_3)\cos(\zeta + \delta_3) - 2\bar{\beta}\cos^2(\zeta + \delta_3)\sin\beta \\ &+ \eta(x_1 + x_2\cos\beta)\cos\delta_3\cos\beta\sin(\zeta + \delta_3) - \eta x_t \sin\delta_3\cos(\zeta + \delta_3) \\ &+ \eta\bar{\beta}^2 x_2\cos\delta_3\sin(\zeta + \delta_3) - 2\eta\bar{\beta}\bar{x}_2\cos\delta_3\cos(\zeta + \delta_3)\sin\beta \\ &+ \frac{\eta g}{\Omega^2 R}\Big\{\Big[\cos(\psi - \delta_3)\sin(\zeta + \delta_3)\cos\beta + \sin(\psi - \delta_3)\cos(\zeta + \delta_3)\Big]\sin\Theta \\ &- \Big[\sin(\psi - \delta_3)\sin(\zeta + \delta_3)\cos\beta - \cos(\psi - \delta_3)\cos(\zeta + \delta_3)\Big]\sin\Phi\cos\Theta \\ &- \sin(\zeta + \delta_3)\sin\beta\cos\Phi\cos\Theta\Big\} + C_{M_D} + \frac{C_{d,L}}{I_h\Omega}\bar{\zeta} + \frac{K_{SL}}{I_h\Omega^2}\zeta = 0 \end{aligned} \quad (22)$$

where

$$C_{M_D} = \int_{x_c}^{1.0} \frac{1}{2}\gamma' u^2 c_{d,o}\cos\phi(x - x_t)dx - \int_{x_c}^{B} \frac{1}{2}\gamma' u^2 c_l \sin\phi(x - x_t)dx \quad (22a)$$

## Flapping Degree of Freedom

The equation of motion for the flapping degree of freedom is obtained by again determining the expanded moment expressions of equation (1). The expressions for moments about the flapping hinge are given in the following sections.

Inertia moment.- The rigid-blade inertia moment about the flapping hinge may be written as

$$M_{I,F} = -\int_{e_1}^{R} m r_F a_F \, dr \tag{23}$$

where $r_F$ is the radial distance from flapping-hinge $Y_F$-axis to mass element, measured in the plane perpendicular to the hinge axis.

By using the same procedure as was described for the acceleration about the lag hinge, the acceleration $a_F$ and the moment arm $r_F$ may be expressed as

$$a_F = \ddot{\beta}(r - e_1)\cos\delta_3 + \Omega^2(r - e_1)\sin\beta\cos\beta + \Omega^2 e_1 \cos\delta_3 \sin\beta \qquad (e_1 \leqq r \leqq e_t) \tag{24a}$$

$$r_F = (r - e_1)\cos\delta_3 \qquad (e_1 \leqq r \leqq e_t) \tag{24b}$$

and

$$\begin{aligned} a_F = {} & \Omega^2(r - e_t)\cos(\zeta + \delta_3)\sin\beta\cos\beta + \ddot{\beta}(r - e_t)\cos(\zeta + \delta_3) - 2\dot{\beta}\dot{\zeta}(r - e_t)\sin(\zeta + \delta_3) \\ & + 2\Omega\dot{\zeta}(r - e_t)\cos(\zeta + \delta_3)\sin\beta + \ddot{\beta}e_2\cos\delta_3 + \Omega^2 e_1\cos\delta_3\sin\beta \\ & + \Omega^2 e_2\cos\delta_3\sin\beta\cos\beta \qquad (e_t \leqq r \leqq R) \end{aligned} \tag{25a}$$

$$r_F = e_2\cos\delta_3 + (r - e_t)\cos(\zeta + \delta_3) \qquad (e_t \leqq r \leqq R) \tag{25b}$$

By substituting equations (24) and (25) into equation (23) and integrating with appropriate limits, the inertia moment may be expressed as

$$\begin{aligned} M_{I,F} = {} & -I_h\Omega^2\cos^2(\zeta + \delta_3)\sin\beta\cos\beta - I_h\ddot{\beta}\cos^2(\zeta + \delta_3) \\ & + 2I_h\dot{\beta}\dot{\zeta}\sin(\zeta + \delta_3)\cos(\zeta + \delta_3) - 2I_h\Omega\dot{\zeta}\cos^2(\zeta + \delta_3)\sin\beta \\ & - 2\frac{M'_W}{g}e_2\Omega^2\cos\delta_3\cos(\zeta + \delta_3)\sin\beta\cos\beta - 2\frac{M'_W}{g}e_2\ddot{\beta}\cos\delta_3\cos(\zeta + \delta_3) \\ & - \frac{M'_W}{g}e_1\Omega^2\cos\delta_3\cos(\zeta + \delta_3)\sin\beta + 2\frac{M'_W}{g}e_2\dot{\beta}\dot{\zeta}\cos\delta_3\sin(\zeta + \delta_3) \end{aligned}$$

$$- 2\frac{M'_W}{g} e_2 \Omega \dot{\zeta} \cos \delta_3 \cos(\zeta + \delta_3) \sin \beta - \frac{W_b}{g} e_2^2 \Omega^2 \cos^2 \delta_3 \sin \beta \cos \beta$$

$$- \frac{W_b}{g} e_2^2 \ddot{\beta} \cos^2 \delta_3 - \frac{W_b}{g} e_1 e_2 \Omega^2 \cos^2 \delta_3 \sin \beta$$

$$- I_e \Omega^2 \cos^2 \delta_3 \sin \beta \cos \beta - I_e \ddot{\beta} \cos^2 \delta_3 - \frac{M'_{W,e}}{g} e_1 \Omega^2 \cos^2 \delta_3 \sin \beta \tag{26}$$

Aerodynamic-force moment.- The expressions for the aerodynamic forces on a blade element are given in equations (5) and (6). From figure 2, the component of these forces (i.e., lift and drag) normal to the blade lag plane is

$$dN = dL \cos \phi + dD \sin \phi \tag{27}$$

The aerodynamic-force moment is therefore

$$M_{A,F} = \int_{r_c}^{R} r_F \, dN \tag{28}$$

where

$$r_F = e_2 \cos \delta_3 + (r - e_t)\cos(\zeta + \delta_3) \tag{28a}$$

By substituting equations (5), (6), and (27) into equation (28), the aerodynamic-force moment may be expressed as

$$M_{A,F} = \int_{r_c}^{BR} \frac{1}{2} \rho U^2 c_l c \cos \phi \left[e_2 \cos \delta_3 + (r - e_t)\cos(\zeta + \delta_3)\right] dr$$

$$+ \int_{r_c}^{R} \frac{1}{2} \rho U^2 c_{d,o} c \sin \phi \left[e_2 \cos \delta_3 + (r - e_t)\cos(\zeta + \delta_3)\right] dr \tag{29}$$

Weight moment.- The components of the gravitational-acceleration vector referred to the shaft axes are given in equation (14). By appropriate coordinate transformations, the gravitational acceleration about the flapping hinge may be shown to be

$$g_F = -g\left[\sin \Theta \cos(\psi - \delta_3) - \sin \Phi \cos \Theta \sin(\psi - \delta_3)\right] \sin \beta - g \cos \Phi \cos \Theta \cos \beta \tag{30}$$

The weight moment about the flapping-hinge axis, defined as positive in the direction of positive $\beta$, is

$$M_{W,F} = \int_{e_1}^{R} mg_F r_F \, dr \tag{31}$$

where

$$\left.\begin{aligned} r_F &= (r - e_1)\cos \delta_3 && (e_1 \leqq r \leqq e_t) \\ r_F &= e_2 \cos \delta_3 + (r - e_t)\cos(\zeta + \delta_3) && (e_t \leqq r \leqq R) \end{aligned}\right\} \tag{31a}$$

By substituting equation (30) into equation (31) and integrating with appropriate limits, the weight moment may be expressed as

$$M_{W,F} = -\left[M'_W \cos(\zeta + \delta_3) + (M'_{W,e} + W_b e_2)\cos \delta_3\right]\left[\cos \Phi \cos \Theta \cos \beta \right.$$

$$\left. + \sin \Theta \sin \beta \cos(\psi - \delta_3) - \sin \Phi \cos \Theta \sin \beta \sin(\psi - \delta_3)\right] \tag{32}$$

Spring-restraint moment.- The spring moment about the flapping hinge is included, as was done for the lag hinge, to permit simulation of structural stiffness or an actual spring at the hinge point. The moment expression is simply

$$M_{S,F} = -K_{SF}\beta \tag{33}$$

Damper moment.- The damper moment is included also for generalization of the rotor system. The moment expression is

$$M_{d,F} = -C_{d,F}\dot{\beta} \tag{34}$$

Flapping equation of motion.- By substituting the five moment expressions derived in the preceding sections (i.e., eqs. (26), (29), (32), (33), and (34)) into equation (1) and by using the nondimensionalizing parameters given in equations (21), the flapping equation of motion may be shown to be

$$\ddot{\bar{\beta}}\left[\cos^2(\zeta + \delta_3) + (\Lambda + \epsilon x_2^2)\cos^2\delta_3 + 2\eta x_2 \cos \delta_3 \cos(\zeta + \delta_3)\right] + \left[\cos^2(\zeta + \delta_3)\right.$$

$$\left. + (\Lambda + \epsilon x_2^2)\cos^2\delta_3 + 2\eta x_2 \cos \delta_3 \cos(\zeta + \delta_3)\right]\sin \beta \cos \beta$$

$$+ \left[(\epsilon x_1 x_2 + \eta_e x_1)\cos^2\delta_3 + \eta x_1 \cos \delta_3 \cos(\zeta + \delta_3) + 2\eta x_2 \bar{\zeta} \cos \delta_3 \cos(\zeta + \delta_3)\right.$$

$$+ 2\bar{\xi}\cos^2(\zeta + \delta_3)\Big]\sin\beta - 2\bar{\beta}\bar{\xi}\Big[\sin(\zeta + \delta_3)\cos(\zeta + \delta_3) + \eta x_2 \cos\delta_3 \sin(\zeta + \delta_3)\Big] - C_{M_T}$$

$$+ \frac{g}{\Omega^2 R}\Big[\eta\cos(\zeta + \delta_3) + (\eta_e + \epsilon x_2)\cos\delta_3\Big]\Big[\cos\Phi\cos\Theta\cos\beta + \sin\Theta\sin\beta\cos(\psi - \delta_3)$$

$$- \sin\Phi\cos\Theta\sin\beta\sin(\psi - \delta_3)\Big] + \frac{C_{d,F}}{\Omega I_h}\bar{\beta} + \frac{K_{SF}}{\Omega^2 I_h}\beta = 0 \qquad (35)$$

where

$$C_{M_T} = \int_{x_c}^{B}\frac{1}{2}\gamma' u^2 c_l \cos\phi\Big[x_2\cos\delta_3 + (x - x_t)\cos(\zeta + \delta_3)\Big]dx$$

$$+ \int_{x_c}^{1.0}\frac{1}{2}\gamma' u^2 c_{d,o}\sin\phi\Big[x_2\cos\delta_3 + (x - x_t)\cos(\zeta + \delta_3)\Big]dx \qquad (35a)$$

## Solution of the Equations of Motion

The equations of motion (eqs. (22) and (35)) are nonhomogeneous and nonlinear with varying coefficients that contain complex integral expressions when such items as stall and compressibility are considered. Thus, it is not feasible to obtain an explicit solution and a numerical iterative method is required.

The procedure used to obtain the results presented is outlined as follows:

1. At an initial azimuth position $\psi_o$, assume initial conditions for $\zeta$, $\bar{\zeta}$, $\beta$, and $\bar{\beta}$.

2. Compute the thrust moment $C_{M_T}$ and drag moment $C_{M_D}$ at the selected azimuth position by evaluating the integrals at specified radial stations and integrating the results by numerical methods.

3. Solve equation (22) for $\ddot{\bar{\zeta}}$ and equation (35) for $\ddot{\bar{\beta}}$.

4. Repeat steps 2 and 3 at the next azimuth position, using values of $\zeta$, $\bar{\zeta}$, $\beta$, and $\bar{\beta}$ obtained by integrating the previously determined quantities $\ddot{\bar{\zeta}}$ and $\ddot{\bar{\beta}}$. Several techniques are available for performing the integration. The method used herein is the Runge-Kutta method described in reference 5.

5. Continue the process at successive azimuth positions until $\beta$ and $\zeta$ reach steady-state values (i.e., repeat for successive rotor revolutions) or one or both of the angles diverge.

The method of solution outlined above yields the transient blade motion from some arbitrary initial condition to a steady-state flight condition. The method may also be

used to compute the transient response of the blade motion due to control inputs or angle-of-attack changes by changing the appropriate input information after the initial steady-state flight condition has been achieved. Rotor-performance characteristics and steady blade motions may also be obtained from the forces and motions computed when the blade motion has reached a steady-state condition. The data presented herein do not cover rotor-performance aspects; however, as an aid in checking the equations and programing, the performance results obtained with this program have been compared with other computer programs (e.g., ref. 2) and very good correlation was found.

## APPLICATION AND DISCUSSION

The applications and results presented herein are intended to illustrate the problems associated with rotor operation at high tip-speed ratios and to define limiting conditions of rotor operation. It must be emphasized that the boundaries presented are for a particular rotor-hub configuration and are not intended to be applicable to all design configurations (e.g., configurations with added hinge restraint and/or dampers). The boundaries presented do, however, indicate the approximate range of tip-speed ratios wherein the destabilizing aerodynamic spring forces will have an adverse effect on blade motion.

The following table lists the primary geometric parameters of the rotor hub and blade which were used in the examples presented herein:

| | |
|---|---|
| $\sigma$ | 0.1 |
| $x_1$ | 0 |
| $x_2$ | 0.05 |
| $x_c$ | 0.2 |
| $C_{d,F}$ | 0 |
| $K_{SF}$ | 0 |
| $C_{d,L}$ | 0 |
| $K_{SL}$ | 0 |
| $\delta_3$ | 0 |
| $\theta_1$ | 0 |
| B | 0.97 |
| $\gamma'$ | Varied as indicated |
| m | Constant (value compatible with $\gamma'$) |

It should be noted that the in-plane damper has been omitted, and consequently, the lag motion will exhibit only the small amount of aerodynamic damping.

The airfoil section characteristics used herein are those given in reference 6. The section characteristics include compressibility effects; however, in order to

minimize such effects on the results presented herein, the rotor tip speed was adjusted to maintain an advancing tip Mach number of 0.8.

## Significance of the Angles $\beta$ and $\zeta$

The hub restraint specified in the derivation of the equations of motion (i.e., lag hinge at or outboard of the flapping hinge) requires the use of a flapping angle $\beta$ which does not directly describe the physical location of the blade. It does, however, give the angular displacement of the flapping-hinge bearing. For example, at extreme lag angles $\zeta$, it is possible to attain a $90^{\circ}$ flapping angle with the blade only slightly out of the hub plane. This may be more clearly illustrated by writing the expression for the blade-tip displacement with respect to the hub plane. From figure 1 the expression for coincident hinges at the center of rotation is simply

$$z_{tip} = R \cos \zeta \sin \beta$$

It is apparent that as $\zeta$ approaches $90^{\circ}$ ($\cos \zeta \rightarrow 0$), the tip displacement approaches zero regardless of the amplitude of $\beta$. Thus, at extreme lag amplitudes, the motion of the flapping hinge must be large for even moderate tip displacement. Since this unique condition exists only at large amplitudes of lag, the flapping angle can generally be considered as a measure of blade motion out of the hub plane for small lag angles (e.g., when $\cos \zeta \approx 1$).

## Stability Examples

Some preliminary applications and results obtained from a numerical solution of the equations of motion derived herein are presented in reference 7. Figure 5 herein, taken from reference 7, shows the blade-motion stability boundaries developed by introducing the same initial flapping-angle displacement at two different initial azimuth positions and solving for the transient blade motions of an unloaded (nonlifting) rotor. The two boundaries illustrate the sensitivity of blade-motion stability to the azimuth position at which a displacement disturbance occurs. It should be noted that the boundaries presented are essentially absolute limits, in that they represent conditions where hinge-motion amplitudes exceed $90^{\circ}$. Consequently, acceptable rotor operation (i.e., hinge-motion amplitudes less than blade mechanical stops) would be limited to tip-speed ratios less than those indicated by the boundaries. In addition, the disturbance amplitude introduced is relatively large and, thus, the lower boundary is in all likelihood conservative. These boundaries, however, were developed for a nonlifting rotor system and it would be expected that the addition of a lifting load would aggravate the condition because lift produces a destabilizing moment. An example of the shift which can occur for a lifting rotor is presented in reference 7.

The fact that stability boundaries may be established over a range of tip-speed ratios for various amplitudes and phasing of the disturbance is significant because it is possible to operate a rotor beyond a specific boundary and then encounter a disturbance of sufficient magnitude to produce a divergent condition.

As a measure of the sensitivity of the boundaries to the initial flapping-angle input, the variation of the limit established for a mass constant $\gamma'$ of 1.6 for varying initial flapping angles is presented in figure 6. The boundary presented was established in the same manner as the boundaries in figure 5. That is, the blade was released from the initial flapping-angle amplitude $\beta_0$ as indicated and the transient solution of the equations of motion was obtained. As indicated in figure 6, the increase in the tip-speed ratio at which unstable motion occurs for decreasing $\beta_0$ is relatively linear for the range $\beta_0 = 0.10$ to $\beta_0 = 0.20$. Below $\beta_0 = 0.10$, the boundary moves more rapidly to higher tip-speed ratios, as might be expected for such small disturbances. Again it should be emphasized that these boundaries are, in effect, absolute limits since the blade amplitudes which occur in the stable region near the boundary are unacceptable in terms of realistic structural limits.

## Limited-Response Boundary

An example of the amplitudes obtained for stable transient motion of the blade near the boundary for $\beta_0 = 0.20$ (presented in fig. 6) is shown in figure 7. The transient motion presented is characteristic of the response obtained when the blade is released with an initial displacement $\beta_0$ at $\psi_0 = 90^\circ$. That is, the flapping angle increases as a result of the negative effective aerodynamic spring in the forward quadrants and the blade swings forward (i.e., leads) as a result of the Coriolis forces resulting from the positive flapping velocity.

The response curve also illustrates another trend which is generally characteristic of the motion for the prescribed initial conditions: for stable conditions near the boundary, the maximum flapping amplitude occurs within the first half revolution after the blade is released. As was pointed out in reference 7, this increase in flapping amplitude occurs because the negative (destabilizing) aerodynamic spring forces in the forward quadrants are larger than the restoring centrifugal spring force. Thus, a more realistic boundary in terms of acceptable rotor operation could apparently be based on the tip-speed ratio at which the restoring spring forces are at least equal to the negative spring forces during the first half cycle after the blade is released at $90^\circ$ azimuth. Thus, upon release of the blade from an initial amplitude, the flapping angles do not exceed the initial amplitude $(\text{i.e., } \beta \leqq \beta_0)$ for the first half cycle. A boundary based on this criterion is presented in figure 8, and represents the approximate tip-speed ratio at which the rotor blade encounters regions of neutral stability in the forward quadrants. Also included is the

absolute limit of figure 5. The area between the two boundaries may be considered as an area of marginal stability. That is, it is an area in which the sensitivity to disturbances is increasing rapidly as a result of the contribution of the destabilizing aerodynamic spring forces in the forward quadrants of the rotor disk.

An example of the blade transient motion which is characteristic of conditions along the lower boundary of figure 8 is presented in figure 9. The significant trend of the transient motion is the relatively flat slope of the flapping amplitude for the first part of the initial revolution as opposed to the large increase shown for the condition presented in figure 7. This relatively flat slope indicates that the nonlinear centrifugal and aerodynamic spring forces are approximately equal for the conditions imposed. In addition, the remaining revolutions indicate that the flapping motion is rapidly damped and that, as expected, the in-plane (lagging) motion has very little damping. The lagging amplitude, however, is not large because the coupling terms (Coriolis forces) are small for the conditions presented.

Since the boundary presented in figure 8 is based on somewhat arbitrary initial conditions, it is of interest to illustrate the significance of the boundary. This was done by establishing a boundary based on a criterion that the maximum flapping does not exceed $15^{\circ}$ when a nonlifting rotor is subjected to a 30-ft/sec (9.14-m/sec) vertical gust. The vertical gust was introduced as a step function in the inflow ratio $\lambda$. The resultant boundary is presented in figure 10 and compared with the boundary of figure 8. It should be noted that the gust input was made with the blade at an initial azimuth angle of zero degrees with zero initial flapping displacement. The agreement between the two boundaries is surprisingly good in view of the fact that they are based on two diverse criteria. In addition, it appears that the boundary based on the criterion of neutral spring forces in the forward quadrants $\left(\beta_{(90-270)} \leqq \beta_0\right)$ gives a very good indication of the tip-speed ratio at which blade-motion stability begins to deteriorate. Thus, the sensitivity to disturbances would probably be of concern when operating at tip-speed ratios above the indicated boundary.

## CONCLUDING REMARKS

The equations of motion for a fully articulated rotor system (flapping and lead-lag degrees of freedom) have been derived and a method for obtaining numerical solutions of the equations is presented. The equations are applicable to a wide range of rotor variables (e.g., airfoil section, twist, root cutout, and hinge geometry) and can account for two-dimensional stall and compressibility effects. The hinge restraints considered require that the lag hinge be coincident with or outboard of the flapping hinge. With this hinge restraint, the flapping angle $\beta$ describes the flapping-hinge motion and does not indicate directly the blade motion with respect to the hub plane.

The equations were used to define blade motion stability boundaries in terms of an absolute limit (i.e., amplitudes greater than $90^{o}$) and to define a boundary based on the criterion of neutral spring forces in the forward quadrants when the blade is released with an initial flapping-angle displacement at an initial azimuth angle of $90^{o}$. The latter boundary is thus a measure of the tip-speed ratio at which the destabilizing aerodynamic spring forces in the forward quadrants are approximately equal to the stabilizing centrifugal forces. Consequently, rotor operation above the boundary could be considered to be in an area of marginal stability in the sense that the rotor sensitivity to disturbances is increasing rapidly. A comparison of the boundary based on the neutral-spring criterion with a boundary based on a maximum flapping-amplitude limit of $15^{o}$ for a 30-ft/sec (9.14 m/sec) vertical gust indicated good correlation.

Langley Research Center,
National Aeronautics and Space Administration,
Langley Station, Hampton, Va., April 5, 1967,
721-01-00-29-23.

## REFERENCES


1. Horvay, Gabriel: Rotor Blade Flapping Motion. Quarterly Appl. Math., vol. V, no. 2, July 1947, pp. 149-167.

2. Jenney, David S.; Arcidiacono, Peter J.; and Smith, Arthur F.: A Linearized Theory for the Estimation of Helicopter Rotor Characteristics at Advance Ratios Above 1.0. Proc. Nineteenth Ann. Natl. Forum, Am. Helicopter Soc., Inc., May 1963, pp. 38-58.

3. Gessow, Alfred; and Crim, Almer D.: A Method for Studying the Transient Blade-Flapping Behavior of Lifting Rotors at Extreme Operating Conditions. NACA TN 3366, 1955.

4. Young, Maurice I.: A Theory of Rotor Blade Motion Stability in Powered Flight. J. Am. Helicopter Soc., vol. 9, no. 3, July 1964, pp. 12-25.

5. Scarborough, James B.: Numerical Mathematical Analysis. Fifth ed., The Johns Hopkins Press, 1962.

6. Tanner, Watson H.: Charts for Estimating Rotary Wing Performance in Hover and at High Forward Speeds. NASA CR-114, 1964.

7. Jenkins, Julian L., Jr.: Calculated Blade Response at High Tip-Speed Ratios. Conference on V/STOL and STOL Aircraft. NASA SP-116, 1966, pp. 17-27.

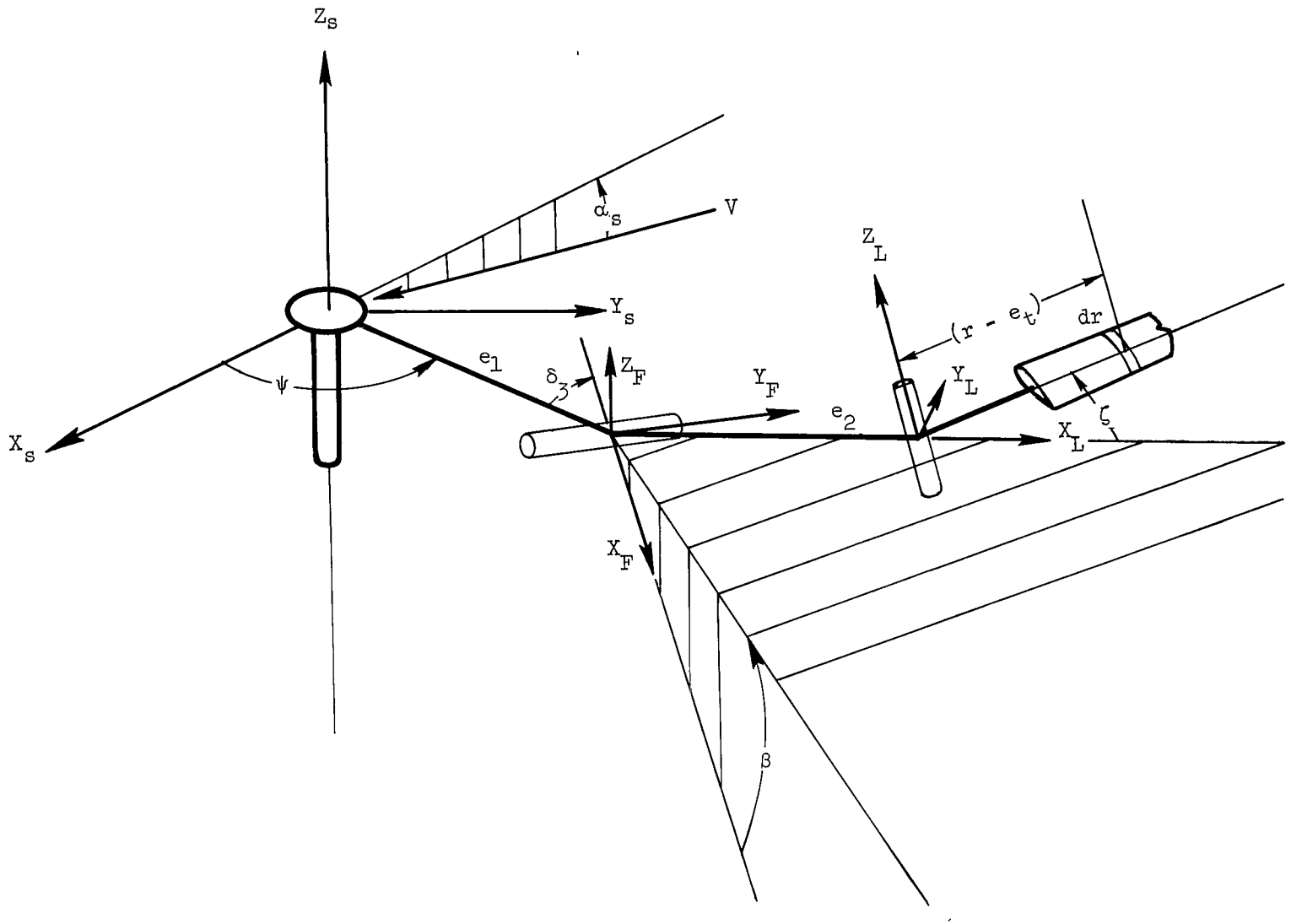


Figure 1.- Geometry of rotor hub.

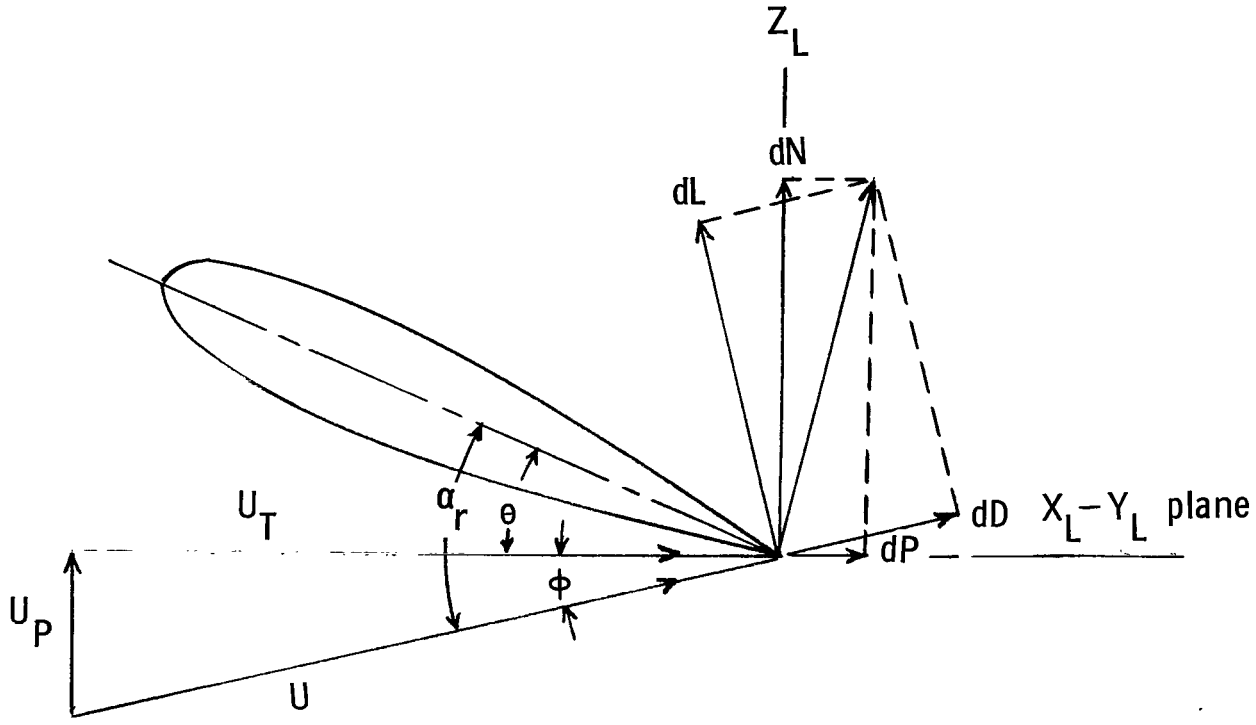


Figure 2.- Forces and angles at the blade element.

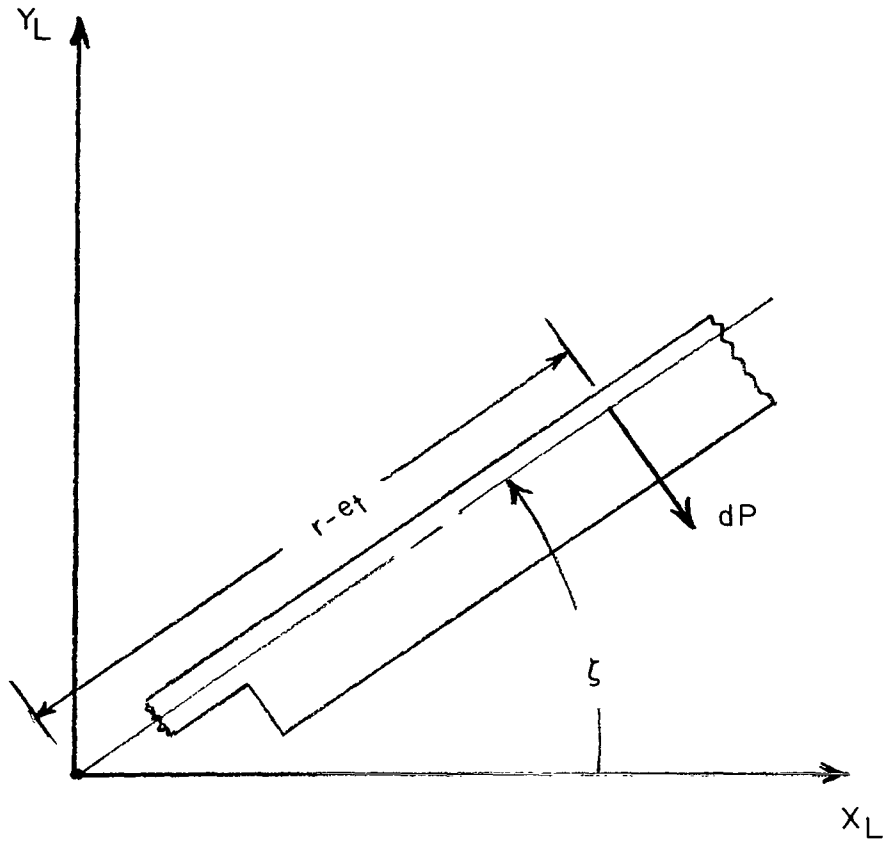


Figure 3.- Component of blade aerodynamic forces producing in-plane moment.

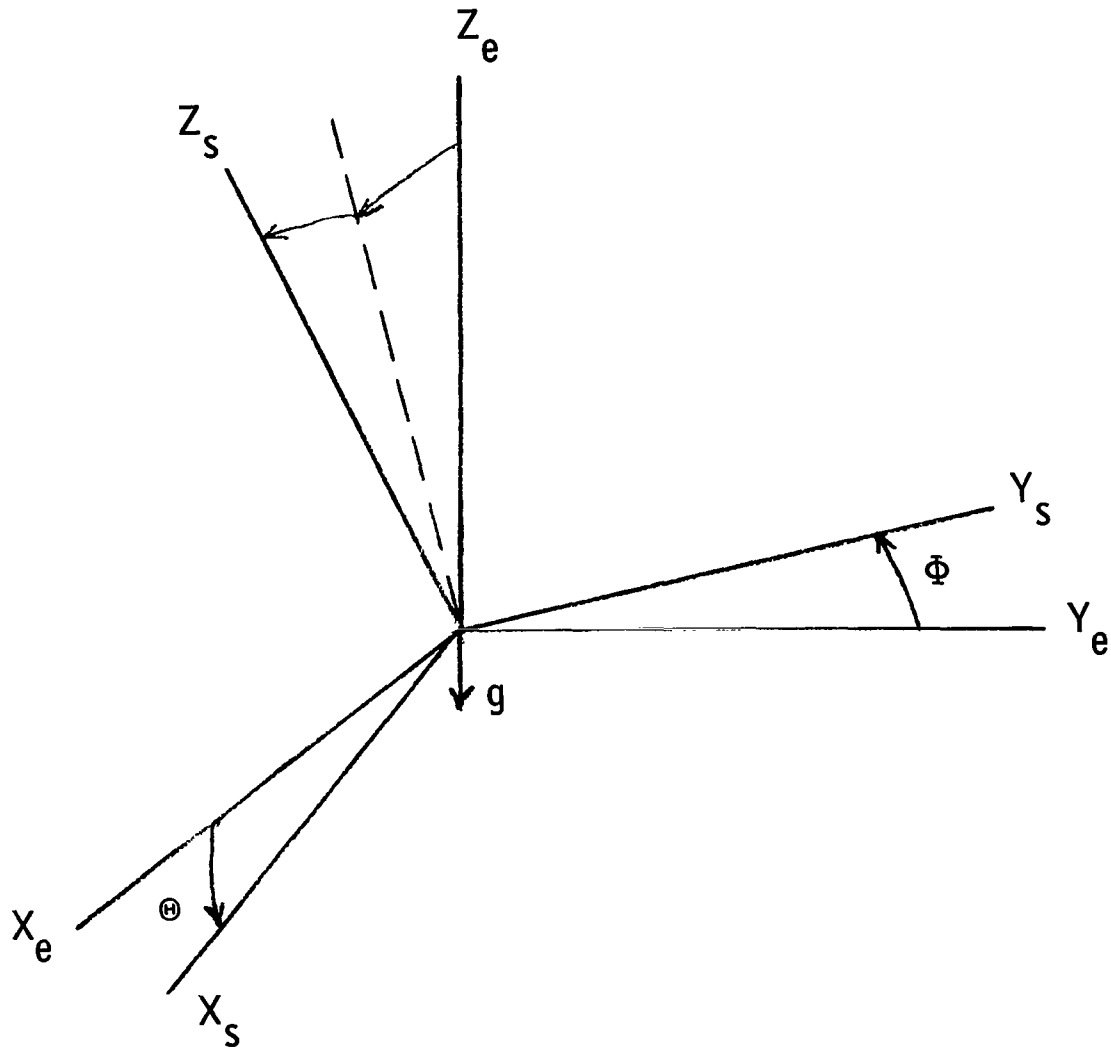


Figure 4.- Orientation of shaft axes with respect to earth reference axes.

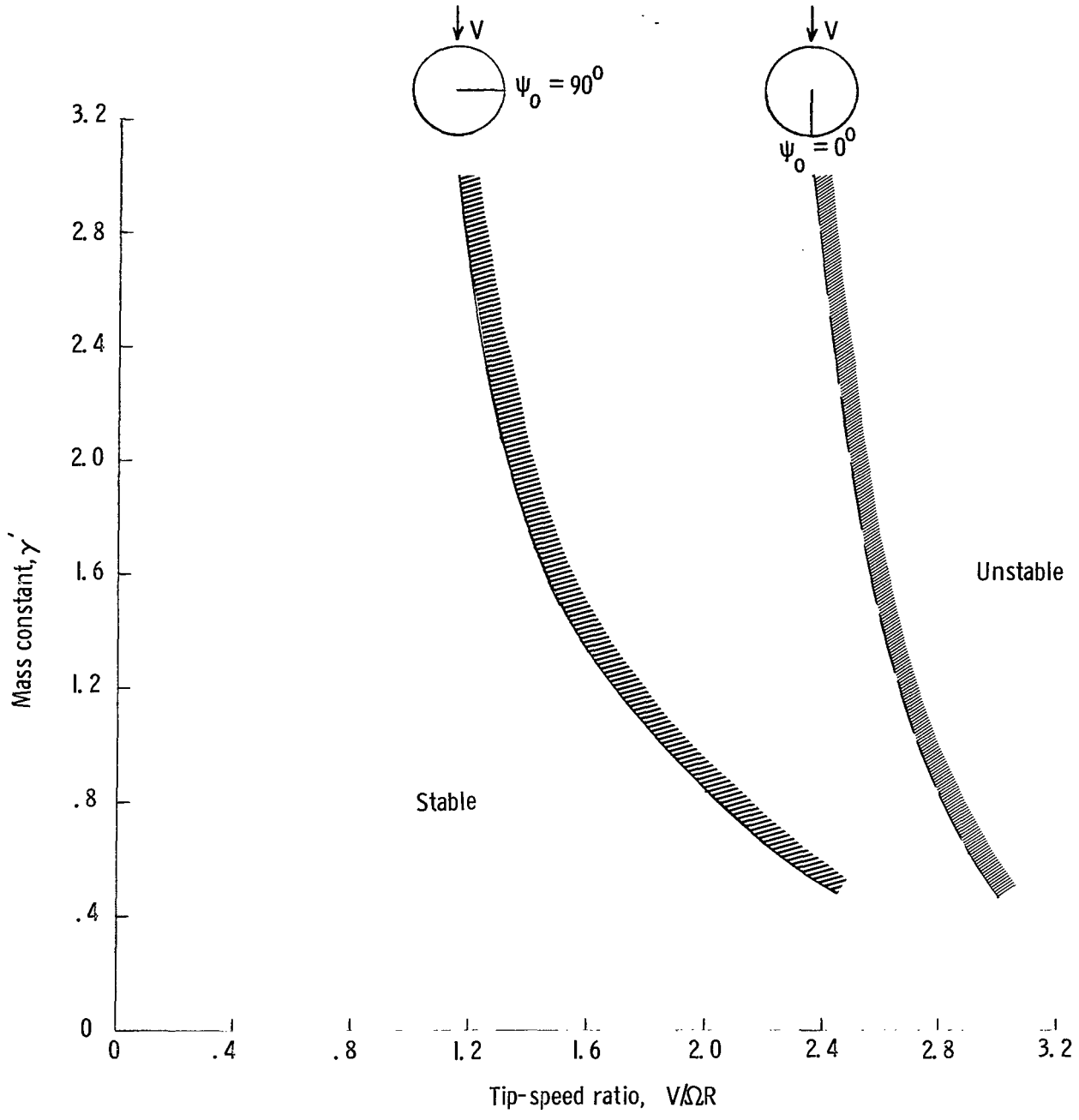


Figure 5.- Effect of initial azimuth angle on blade-motion stability boundary. $\beta_0 = 0.2$ rad.

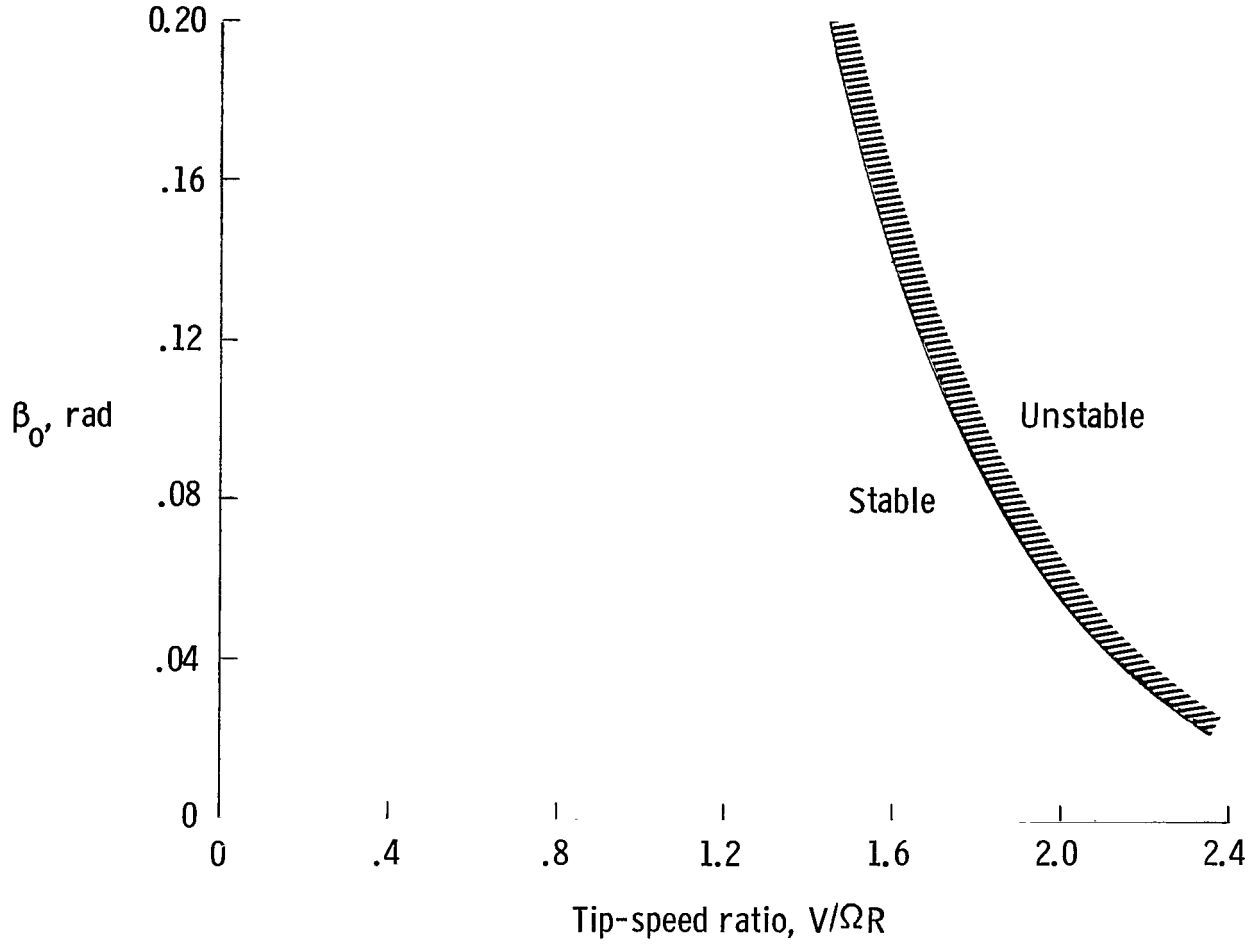


Figure 6.- Effect of initial flapping-angle displacement $\beta_0$ on blade-motion stability. $\psi_0 = \pi/2$ rad; $\gamma' = 1.6$.

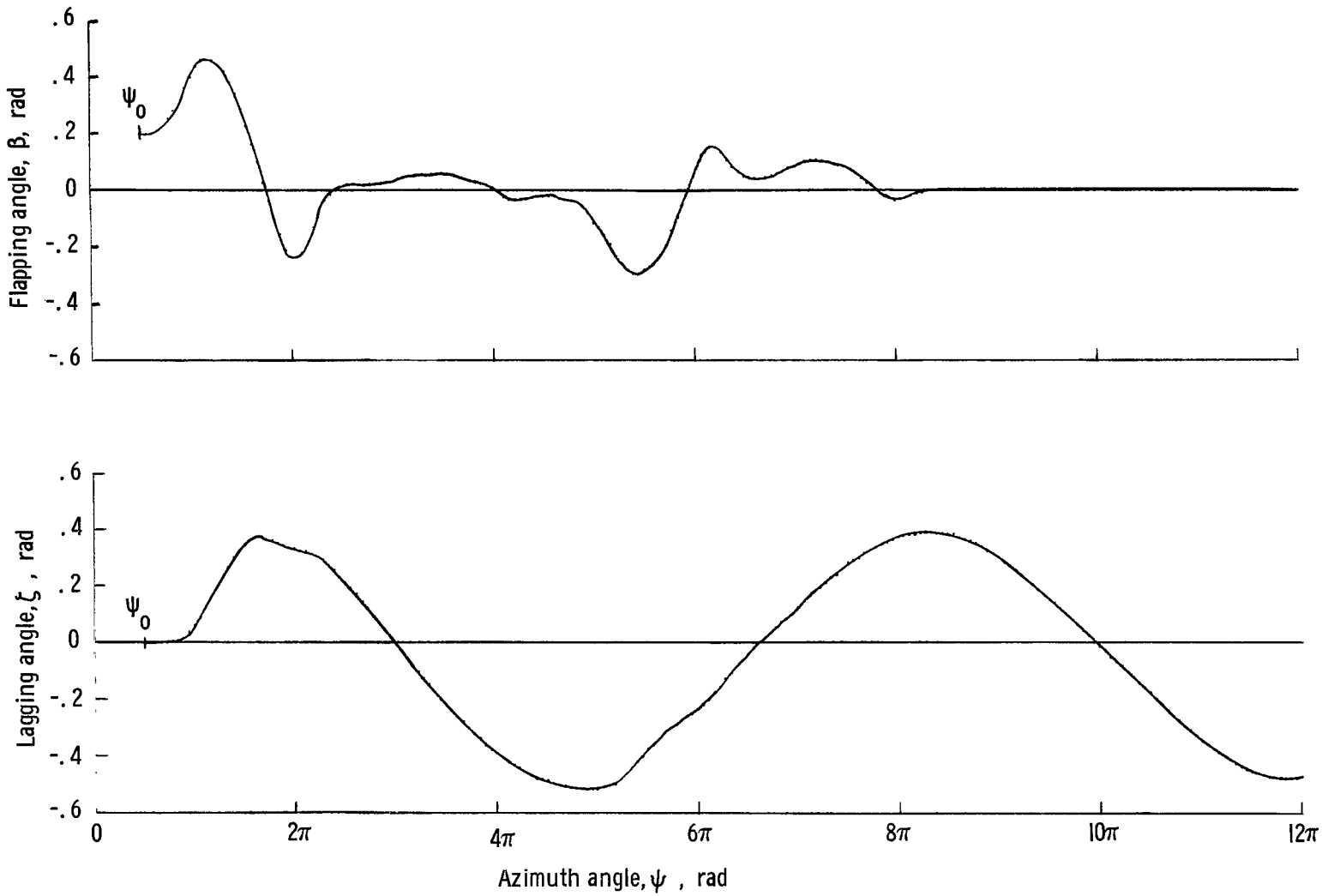


Figure 7.- Transient motion near unstable boundary. $V/\Omega R = 1.4$; $\gamma' = 1.6$.

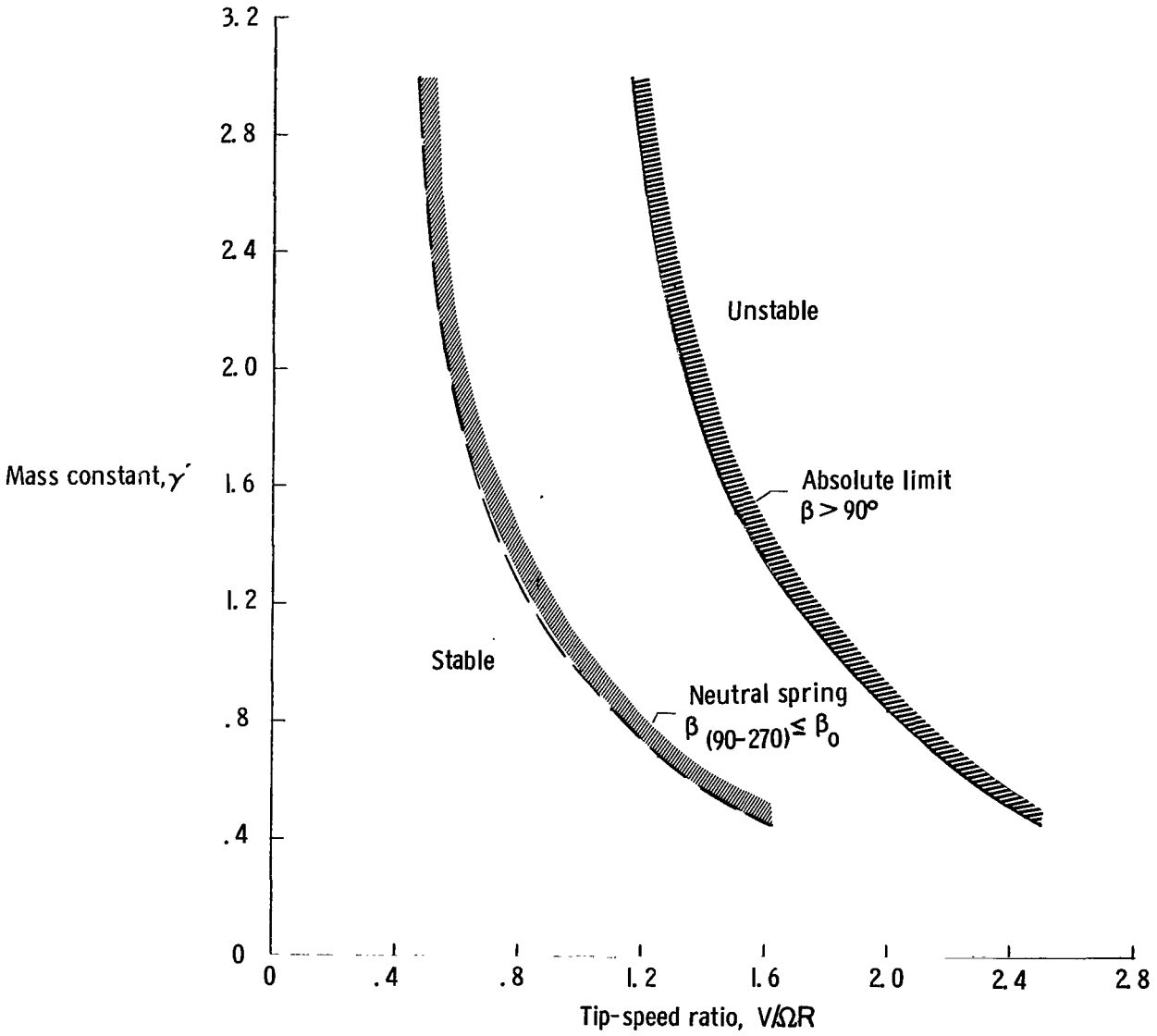


Figure 8.- Comparison of boundary based on neutral spring forces in forward quadrants with absolute-limit boundary. $\psi_0 = \pi/2$ rad; $\beta_0 = 0.2$ rad.

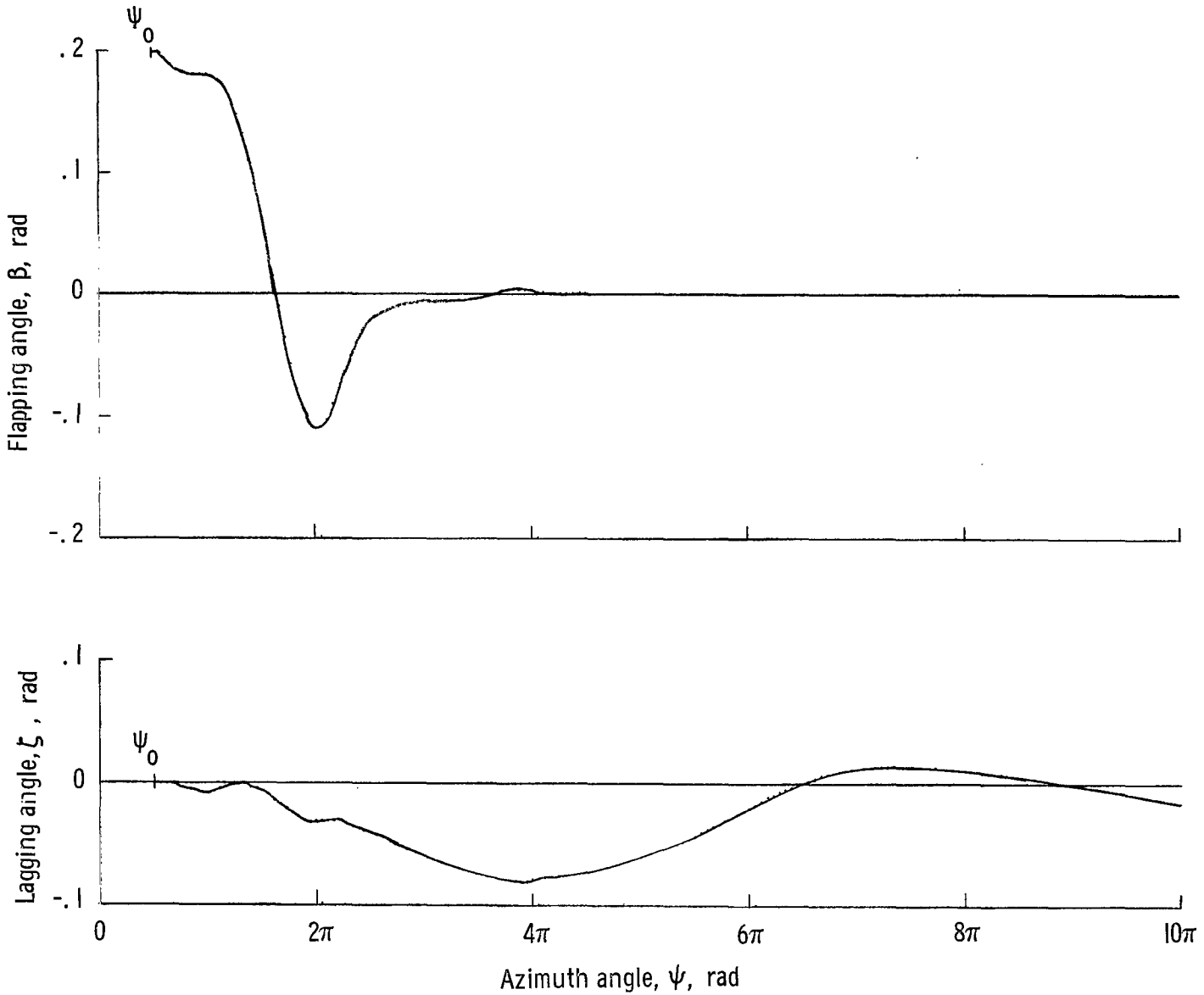


Figure 9.- Transient motion at boundary of neutral spring forces in forward quadrants. $V/\Omega R = 0.6$; $\gamma' = 1.6$.

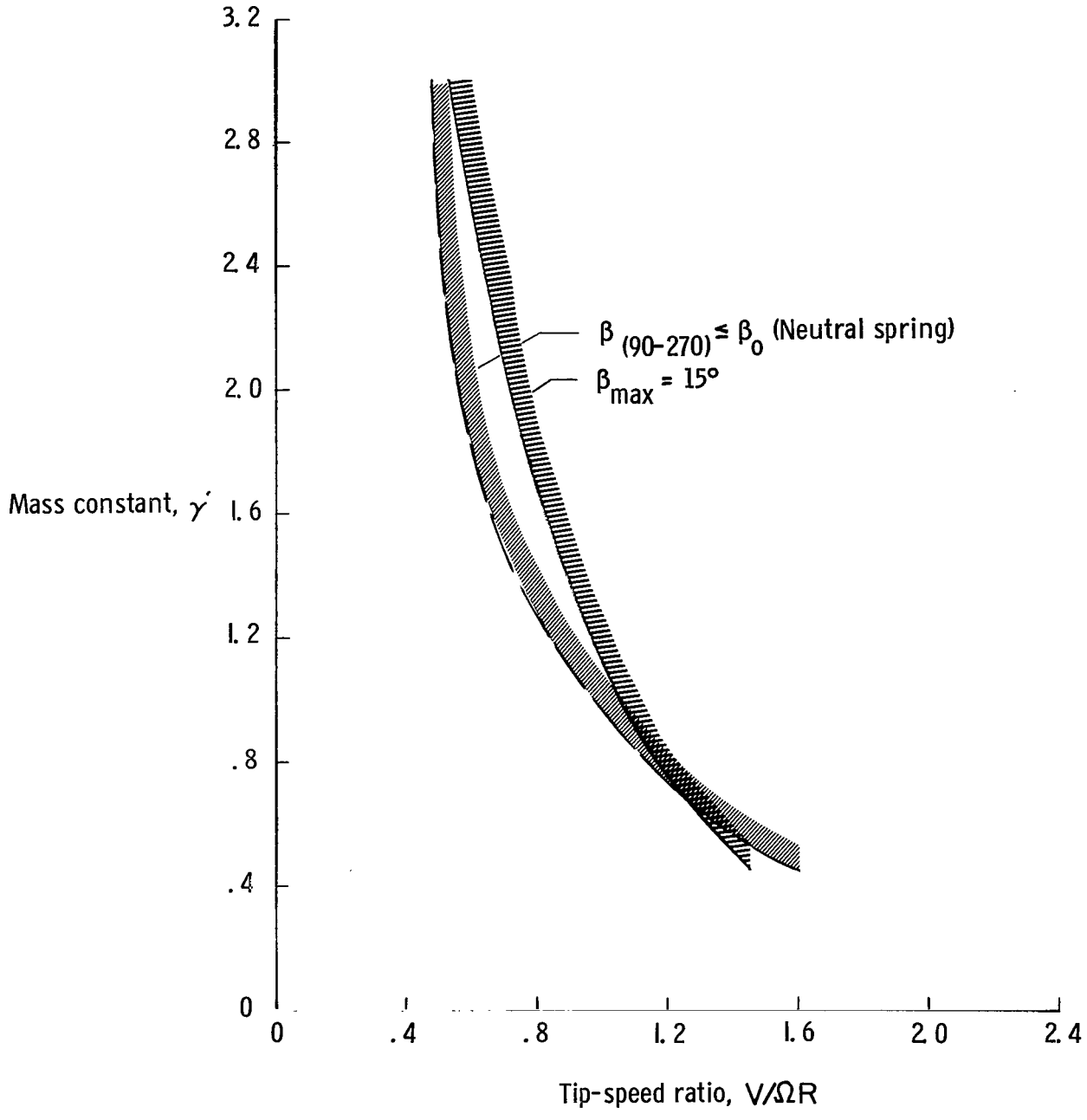


Figure 10.- Comparison of neutral-spring-force boundary with blade-flapping-amplitude boundary.

*"The aeronautical and space activities of the United States shall be conducted so as to contribute . . . to the expansion of human knowledge of phenomena in the atmosphere and space. The Administration shall provide for the widest practicable and appropriate dissemination of information concerning its activities and the results thereof."*

—NATIONAL AERONAUTICS AND SPACE ACT OF 1958

# NASA SCIENTIFIC AND TECHNICAL PUBLICATIONS

TECHNICAL REPORTS: Scientific and technical information considered important, complete, and a lasting contribution to existing knowledge.

TECHNICAL NOTES: Information less broad in scope but nevertheless of importance as a contribution to existing knowledge.

TECHNICAL MEMORANDUMS: Information receiving limited distribution because of preliminary data, security classification, or other reasons.

CONTRACTOR REPORTS: Scientific and technical information generated under a NASA contract or grant and considered an important contribution to existing knowledge.

TECHNICAL TRANSLATIONS: Information published in a foreign language considered to merit NASA distribution in English.

SPECIAL PUBLICATIONS: Information derived from or of value to NASA activities. Publications include conference proceedings, monographs, data compilations, handbooks, sourcebooks, and special bibliographies.

TECHNOLOGY UTILIZATION PUBLICATIONS: Information on technology used by NASA that may be of particular interest in commercial and other non-aerospace applications. Publications include Tech Briefs, Technology Utilization Reports and Notes, and Technology Surveys.

*Details on the availability of these publications may be obtained from:*

SCIENTIFIC AND TECHNICAL INFORMATION DIVISION

NATIONAL AERONAUTICS AND SPACE ADMINISTRATION

Washington, D.C. 20546